Arabian Journal of Geosciences (2024) 17:180
https://doi.org/10.1007/s12517-024-11983-8

ORIGINAL PAPER

Crustal deformation from GNSS measurement and earthquake mechanism along Pieniny Klippen Belt, Southern Poland

Kutubuddin Ansari[1] · Janusz Walo[1] · Andrean V. H. Simanjuntak[2] · Kinga Wezka[1]

Received: 13 March 2023 / Accepted: 2 May 2024

Abstract

The dynamic geological features of the Pieniny Klippen Belt (PKB) in southern Poland are nowadays a focal point of researchers as it is recognised as an active zone of crustal discontinuity. In the present study, we employed long-term analysis of ground-based global navigation satellite system (GNSS) measurements (from 2004 to 2020) to probe the crustal deformation, strain rates, and rotational rates in the PKB unit and the surrounding region, i.e., Magura Nappe (MN) and Podhale Flysch (PF) units. Measured velocities from GNSS observables are modelled by the auto-regressive integrated moving average (ARIMA) method to comprehend the long-term tectonic deformation. Our results showed that the ARIMA-modelled velocity varied from ~ 0.15 to ~ 8.86 mm/yr, indicating about 8.71 mm/yr difference along all units. Such differences suggest that crustal slip along the active thrusts and folds is the major factor causing regional deformation. The strain rates in PKB are also varying from the western to the eastern part. The rotational rates in PKB show a counterclockwise (CCW) pattern similar to the strain rates. These patterns suggesting that the PKB was rotated in the CCW direction with a large angle during the Miocene period. Finally, we analysed the seismicity for a period from 2004 to 2020 by using Bayesian moment tensor inversion and multivariate Bayesian inversion. The Bayesian inversion was applied based on bootstrapping chain analysis to figure out the earthquake mechanism using moment tensor inversion for the mainshock that occurred in Poland on 20 July 2018. The inversion results for the 2018 earthquake resolved a thrusting mechanism with nodal plane-1 having a strike of 346°, dip of 32°, and rake of 92° and a nodal plane-2 with a strike of 163°, dip of 58°, and rake of 89°. Since the seismicity in the Poland region has experienced less significant earthquakes in the last century, it is reasonable to attribute this lower seismic activity to the correspondingly low slip rates discerned through geodetic monitoring efforts.

Keywords The Pieniny Klippen Belt · Magura Nappe · Podhale Flysch · GNSS · Seismicity

Introduction

The regional area of Poland is a part of central Europe located within the three major tectonic continental scales such as Variscan West European Platform (WEP) terranes in the southwest, Precambrian East European Craton (EEC) to the northeast, and Alpine Carpathian arc (younger) in the south (Grad et al. 2016). The EEC western and southern margins are marked as the Teisseyre Tornquist Zone (TTZ) inside Poland which is associated with the southwestern edge of the paleocontinent Baltica (Dadlez et al. 2005; Bogdanova et al. 2006) (Fig. 1). The TTZ is a linear feature, and major lithospheric structure considered to be a deep-seated boundary up to a depth of about 200 km, marked in the southwestern boundary of the EEC (Bruneton et al. 2004; Wilde-Piórko et al. 2010). Tectonically, the TTZ is the largest feature in Europe which separates the old thick EEC Palaeozoic sedimentary crust and the younger thin Phanerozoic mobile belts crust in central and western Europe. The deep-seated nature of TTZ was indicated by several hundred seismic events and explosions in Europe (Lizurek 2017). Although Poland experiences less seismicity and significant earthquakes, there are 100 significant earthquakes that occurred mainly in the southern part of Poland since 1000 A.D. (see the

Responsible Editor: Longjun Dong

✉ Kutubuddin Ansari
kdansarix@gmail.com

[1] Faculty of Geodesy and Cartography, Warsaw University of Technology, Warsaw, Poland

[2] Agency for Meteorology, Climatology, and Geophysics (BMKG), Jakarta, Indonesia

Published online: 16 May 2024

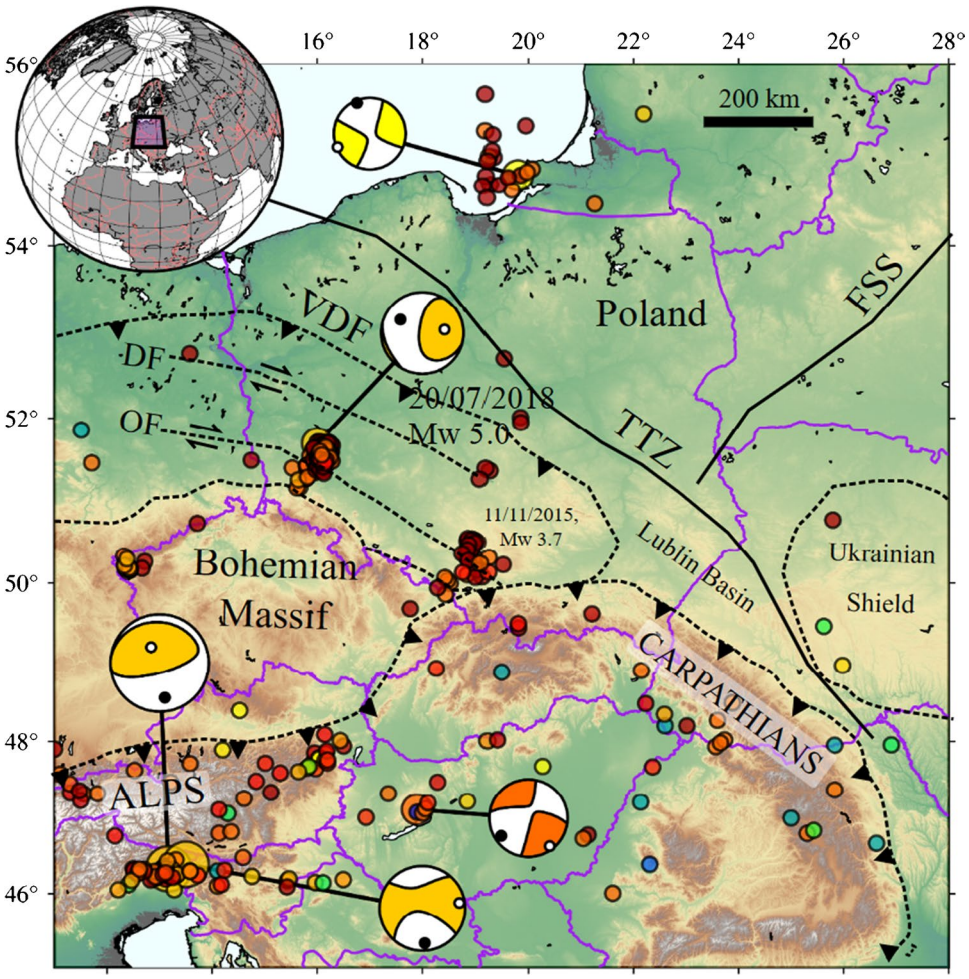

Fig. 1 The tectonic map of Poland and historical seismicity. There are two clusters (11 Nov 2015 and 20 Jul 2018) of felt earthquakes occurred in the last decade. The earthquake data was taken from International Seismological Centre (ISC) and Global Centroid Moment Tensor (GCMT). The short names are like this: Variscan Deformation Front (VDF), Fennoscandia–Sarmatia Suture (FSS), Dolsk Fault (DF), Odra Fault (OF), and Teisseyre Tornquist Zone (TTZ)

Table S1, supplementary file for the list of recorded earthquakes). The southern part of Poland has a more active tectonic system where the greatest earthquake in Poland occurred on 3 December 1786, with an approximated magnitude of around ~ 5.6 ML. The Podhale earthquake occurred on 30 November 2004 with a magnitude of ML 4.8 was categorised as the biggest earthquake event in Poland that was recorded by the modern seismometer network (Wiejacz and Dębski 2009). There are some magnitude earthquakes near Krynica recorded (Guterch et al. 2005; Plesiewicz and Wiszniowski 2015) and later in 2007 near Jarocin (Lizurek et al. 2013). The main source of the seismic activity occurring in the southwestern part of Poland is related to industrial happenings such as mining in the underground Upper Silesian Coal Basin (USCB) and Legnica Głogo Copper District (LGCD). Several hundreds of annual seismic events are mainly produced by these seismic events with magnitudes up to 4.5 ML (Lasocki 2005). The largest earthquakes in this region were ML 4.5 on 24 March 1977, ML 4.3 on 20 June 1987, and ML 4.2 on 19 March 2013 (Gibowicz et al. 1989, Lizurek et al. 2015, Rudziński et al. 2016).

The Pieniny Klippen Belt (PKB) with a very complex geological structure is a remarkable zone in the southern part of Poland (Birkenmajer 1974, 1986). The exact location of PKB has been shown with a red rectangle in Fig. 2. The boundaries of PKB lie between the Inner and Outer Carpathians structural units in the south and north respectively and directly adjacent to the Magura Nappe (MN) (Zuchiewicz 1995; Jurewicz 2005). The tectonic phenomenon of PKB is very complicated resulting from the progressions started from the Alpine orogeny. The PKB sediments structures are mainly folds and horsts created during the period of Jurassic and Cretaceous in an ocean basin and make Western Tethys northern part. The compression from the south during the time of the Cretaceous caused scaling, refolding, and boudinage of the nappe structure (Birkenmajer 1974). The complicated geological structure of the PKB remained of great interest to geodynamical researchers for a long time. Geodynamic research has been done from the 1960s until now (Ząbek et al. 1988, 1993; Margański 1997; Barlik 1998; Czarnecki et al. 2005; Walo et al. 2016). The neo-tectonic activity was noticed during the 1960s, and the block-like nature of vertical movements was detected during

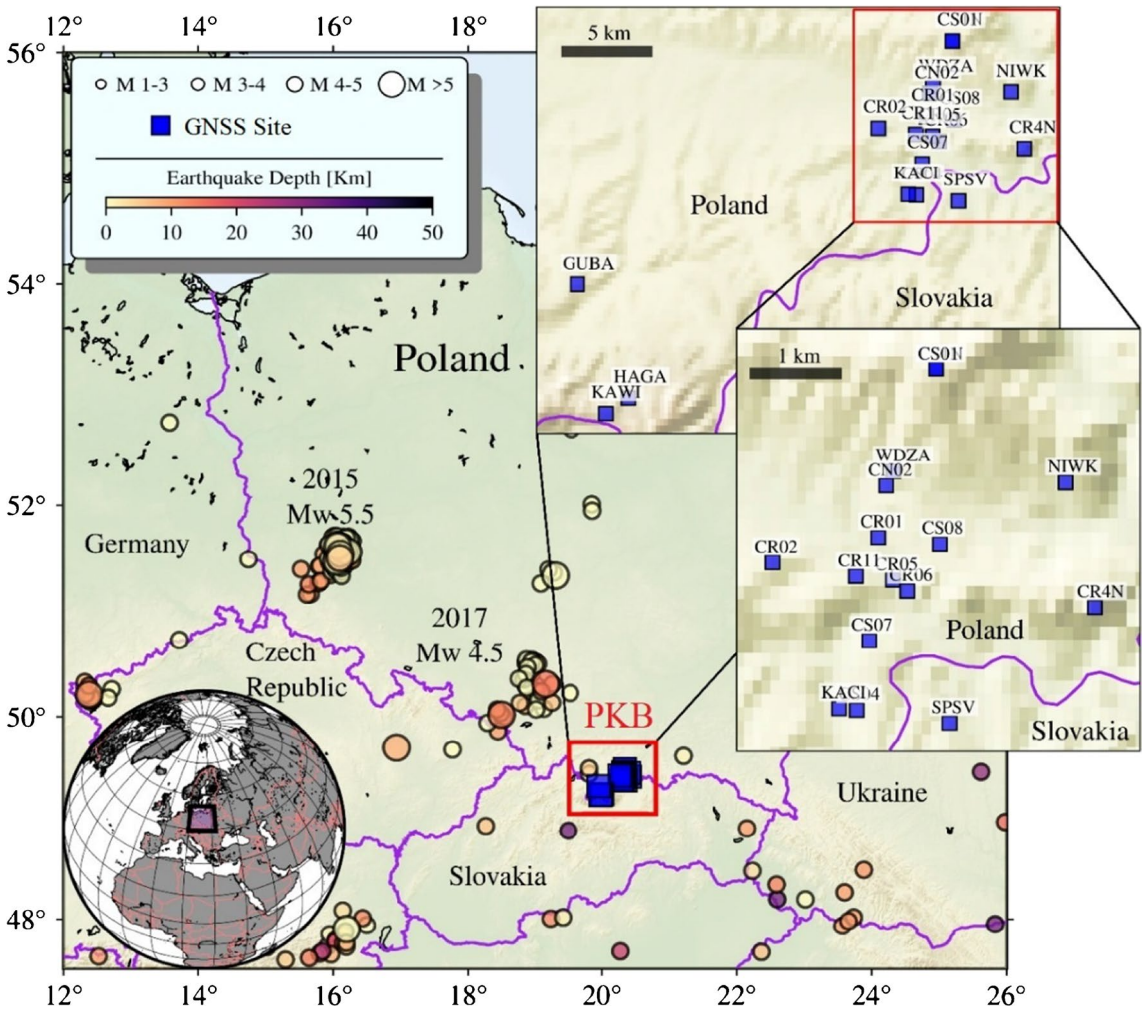

Fig. 2 The Global Navigation Satellite System (GNSS) network (rectangular blue) in the Pieniny Klippen Belt (PKB). The circle represents epicentre of the earthquake occurrence in southern Poland

1978–1995 in PKB (Ząbek et al. 1988, 1993; Margański 1997; Barlik 1998). An innovative investigation aspect of the PKB tectonic activity was created during the 1990s because of the newly built Dunajec river dam and reservoirs of water in Sromowce Wyzne and Czorsztyn. There are notable changes in the PKB vertical movement with respect to neighboring Magura Nappe (MN) and Podhale Flysch (PF) seen during 2001–2003 measurements (Czarnecki et al. 2005). The results of geodynamic examinations during 2004–2015 indicate that the PKB exhibits minor neotectonics activity mainly in the vertical movement while the horizontal movements were minor without clear tendencies in the magnitude and direction (Walo et al. 2016).

The analysis of soil texture and the content and lithology of rock fragments indicate discontinuities in the parent material of the upper and lower sections of the investigated profiles (Kacprzak and Derkowski 2007). There are numerous snail shells representing various ecologic groups, and the diversification of the assemblages reflects the mosaic pattern of their habitats in the initial limestone soil, which were being slightly changed by human impact (Alexandrowicz 1993). In the Pieniny Mountains, being the highest part of the Klippen Belt in the Carpathians, four important soil profiles are located. The area is characterised by complex, mosaic-like lithology with a large contribution of carbonate rocks, mainly limestones, surrounded by other sedimentary rocks such as shales, siltstones, and sandstones (Kacprzak and Derkowski 2007). Limestones usually form isolated hills or short ridges with steep slopes. Rendzic Leptosols and Calcaric Leptosols dominate the soil cover. They are usually surrounded by Eutric Leptosols, whose genesis and properties have commonly been attributed to the characteristics of bedrock containing less limestone (Niemyska-Lukaszuk et al. 2002). Kacprzak and Derkowski (2007) noticed the differences in the spectra for the whole, unseparated soil material as well as the N2 μm fraction (detrital minerals) demonstrates the

occurrence of a discontinuity between bedrock and/or saprolite and cover-beds and are confirmed by differences of soil texture and lithology of rock fragments. They believed that the specific properties of the described group of Eutric Cambisols in the Pieniny Mountains, i.e., contrasts in carbonate content and pH, also result from the contrast between redeposited, allochtonous hillslope sediments (cover-beds) and the underlying bedrock. Cover-beds should be recognised as the parent material for the upper sections of the investigated profiles, whereas the properties of bottom sections are strongly related with underlying bedrock. Moreover, Carpathian soils characterise low rates of decomposition of plant material because of cool and humid conditions as well as adjacent plant communities and soil organisms (Drewnik 2006). The Sobótka Limestone Member displays unusual succession of calpionellids and is terminated by uneven palaeokarstic surface dominated by hummocky karren forms with rounded tops which are typical for karst evolved under thick soil cover. The karstic surface is covered by a condensed succession of the Late Albian red pelagic marly limestones and marlstones (Chmielowa Formation). The stratigraphic gap encompasses a time span from the Berriasian to the Late Albian (Jamrichová et al. 2012).

The time series obtained from GNSS have been used to investigate the hydrological loading, glacial isostatic adjustment, and pre-seismic, coseismic as well as post-seismic deformation due to earthquakes in different regions of the world (Mukul et al. 2014; Ansari et al. 2017; Mukul et al. 2018; Ansari and Park 2019, 2022; Ansari and Bae 2020; Qi et al. 2023). Although a significant number of studies related to the geodynamic motion of PKB and the surrounding region have been done based on high-precision positioning, however, there is significant space for exploring the current and past neotectonics activities, which will help to understand the complicated geological structure of PKB and surrounding region in Southern Poland. Therefore, in the current study, we used 18 global navigation satellite system (GNSS) campaign mode GNSS stations located in PKB and surrounded regions of 16 years (2004–2020) observations and studied the active deformation to improve the current understanding of tectonic activities in the PKB (Fig. 2). In this network, five stations from MN and six stations from PF are included (Fig. 3). Mainly two types of surveying set observations are accomplished: a Leica GX1230GG receiver with the LEIAX1202GG antenna and Trimble 4007 receiver with the Trimble Micro-Cantered L1/L2 + GP antenna. These GNSS data in RINEX format have been processed by GAMIT-GLOBK (GNSS Analysis at MIT and Global Kalman Filter) post-processing software (Herring et al. 2018), and their daily precise point positioning

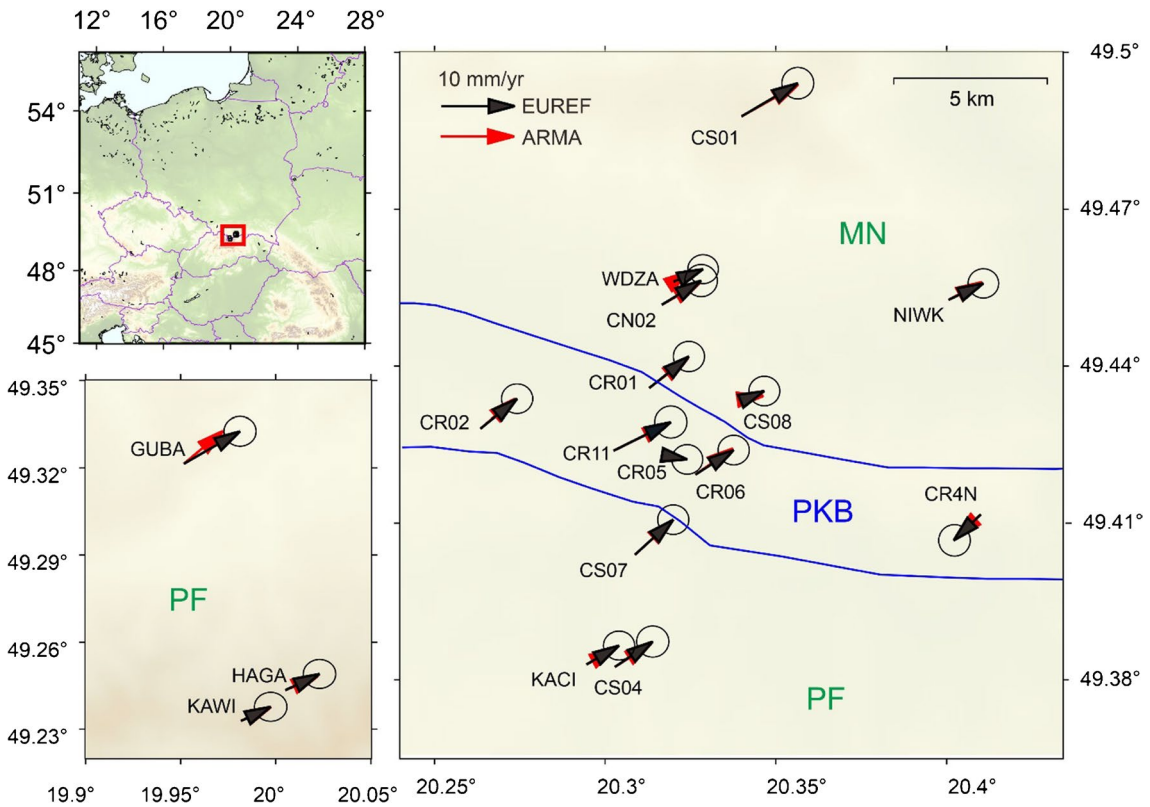

Fig. 3 EUREF- and ARIMA-predicted velocity field in PKB zone from 2004 to 2020

(PPP) are estimated. The method of differential phase observation was utilised to estimate the coordinates of GNSS stations, orbital parameters of satellites, phase ambiguity, and ionospheric and tropospheric delays. Daily precise position measurements of GNSS sites are estimated with respect to Eurasia-Fixed Reference Frame 2014 (EUREF 2014) along with the 95% confidence interval (Fig. 3; Table 1). The loose constraint of GNSS solutions obtained from GAMIT is combined in GLOBK with daily solutions of available International GNSS Service (IGS) stations namely BOGI, JOZE, LAMA, BOR1, and WROC in Poland. This kind of network solution indicated high-accuracy results in the current study. Basically, the whole study has been divided in three steps. In the first step, these EUREF velocities are modelled with ARIMA method, then both observed and modelled velocities are used to study the behaviour of crustal deformation in PKB. In the second step, we estimated strain and rotation rate of GNSS velocities and compared their results with previous published results. Finally, we analysed the earthquake mechanism that occurred in the Lower Silesia province on 20 July 2018 using moment tensor inversion for the mainshock and largest aftershock with the seismic stations from Geofone Seismic Network.

Methodology of GNSS studies in PKB

We assumed that the GNSS station shifted linearly or in a periodic way during the data collection. To eliminate the seasonal changes, the measurements were always made at the same time of year (first half of September). Some kind of natural phenomenon such as snow, rainfall, ups and downs of temperature, and partial correction of tropospheric and ionospheric delays may cause random errors in signals. These kinds of errors in signal affect the secular tectonic deformation measurements (Li et al. 2000). There are several kinds of models developed to remove such kinds of errors and present the secular tectonic deformation. Auto-regressive integrated moving average (ARIMA) is one of them which has been successfully applied for the north, east, and up components of GNSS positions in different places (Li et al. 2000; Ansari 2018). The obtained results indicate that the ARIMA model is able to extract valuable information from GNSS measurements after removing the discontinuities in the time-series. The mathematical summary of the ARIMA model working principle is as follows:

If v indicates the stationary time-series of GNSS velocities, then the ARIMA forecasting equation for them is given by the following:

$$\text{Forecasting of } v \text{ at time } t = \text{sum of last } p - \text{weighted values of } v + \text{sum of last } q - \text{weighted forecast errors} + \text{constant}$$

Table 1 EUREF and ARIMA modelled velocity of selected GNSS stations in PKB and surrounding region

GNSS site name	Location	EUREF velocity				ARIMA modelled		
		Vel (E) (mm/yr)	Vel (N) (mm/yr)	Magnitude (mm/yr)	Azimuth (°N)	Vel (E) (mm/yr)	Vel (N) (mm/yr)	Magnitude (mm/yr)
CN02	49.452° N; 20.317° E	5.35 ± 1.03	3.3 ± 1.02	6.29	58.33	5.15	2.97	5.95
CR01	49.435° N; 20.313° E	5.41 ± 0.99	4.3 ± 0.96	6.91	51.52	5.29	4.07	6.67
CR02	49.428° N; 20.263° E	4.99 ± 0.99	4.06 ± 0.94	6.43	50.87	4.69	4.04	6.19
CR04	49.414° N; 20.414° E	0.14 ± 1.00	0.10 ± 1.00	0.17	54.46	0.12	0.09	0.15
CR05	49.423° N; 20.320° E	2.01 ± 0.98	− 0.36 ± 0.94	2.04	100.15	0.14	− 0.36	0.39
CR06	49.419° N; 20.326° E	5.21 ± 0.99	3.34 ± 0.94	6.19	57.34	5.10	3.57	6.23
CR11	49.424° N; 20.302° E	7.81 ± 1.02	3.9 ± 1.01	8.73	63.46	7.57	3.72	8.43
CR4N	49.414° N; 20.414° E	− 3.89 ± 0.99	− 2.62 ± 1.02	4.69	236.04	− 3.89	− 2.62	4.69
CS01	49.488° N; 20.340° E	7.68 ± 1.01	4.54 ± 1.00	8.92	59.41	7.72	4.35	8.86
CS04	49.382° N; 20.303° E	5.16 ± 1.02	3.46 ± 0.99	6.21	56.15	4.94	3.14	5.85
CS07	49.404° N; 20.309° E	5.22 ± 0.99	4.78 ± 0.94	7.08	47.52	5.14	4.69	6.96
CS08	49.434° N; 20.342° E	2.26 ± 0.98	0.97 ± 0.94	2.46	66.77	2.12	0.31	2.14
GUBA	49.321° N; 19.952° E	7.65 ± 1.02	4.42 ± 0.94	8.84	59.98	5.34	4.49	6.98
HAGA	49.243° N; 20.005° E	4.63 ± 1.03	2.22 ± 0.92	5.13	64.38	4.42	1.95	4.83
KACI	49.383° N; 20.294° E	4.45 ± 0.99	2.58 ± 0.92	5.14	59.89	3.99	2.11	4.51
KAWI	49.233° N; 19.982° E	4.06 ± 1.03	1.93 ± 0.92	4.49	64.57	4.12	1.91	4.54
NIWK	49.453° N; 20.401° E	4.75 ± 0.97	2.25 ± 0.93	5.26	64.65	4.58	2.42	5.18
WDZA	49.456° N; 20.320° E	4.04 ± 0.97	1.71 ± 0.92	4.39	67.06	2.24	1.44	2.66

Where "p" and "q" are known as weighted coefficients. The p and q are small negative or positive integers and, in most cases, either p or q are taken equal to zero. The sum of $p+q$ is considered equal to 3 or sometimes less than 3. In this condition, the right-side equation will not contain too many terms. The value of the constant term can be or cannot be taken as zero.

The lagged terms of v in the visible equation are called "autoregressive" (AR) and the lagged terms of the forecast errors are known as "moving average" (MA). The forecast value of v into t-1 to t time-period based on the data observable can be written like below (Nau 2014):

$$\hat{v}_t = \mu + \phi_1 v_{t-1} + ... + \phi_p v_{t-p} - \theta_1 e_{t-1} - .... - \theta_q e_{t-q} \quad (1)$$

where μ is the term of constant, ϕ_k and θ_k are the AR and MA coefficients respectively at lag k. The value $e_{t-k} = v_{t-k} - \hat{v}_{t-k}$ is the forecasting error which was equipped at period t-k (Nau 2014).

The ARIMA model equation in mathematical form can be given as follows:

$$\hat{v}_t = \mu + \sum_{i=1}^{p} \phi_i v_{t-i} - \sum_{j=1}^{q} \theta_j e_{k-1} \quad (2)$$

The intention of this kind of forecasting of long-term GNSS time-series is to remove the noise error during the data collection and positioning measurement. After removing the error, we found modelled velocity which better helps to investigate the secular crustal deformation and strain analysis in a given region. In the current study, we selected the ARIMA model (with order $p=1$ and $q=1$) and tried to forecast the velocity values in the PKB region. The preliminary results of the study showed that the ARIMA model is an effective tool for studying tectonic activities in the selected region.

We carried out strain analysis in the study area by applying the zero_strain programme of a 2D version (Teza and Galgaro 2008). In this programme, it has been assumed that the initial coordinate of the geodetic network is given by (x, y). If the coordinates of the original network shift (Δx, Δy) during the repeated measurement, then the rectilinear functions shift coordinate (u, v) in the 2D system can be specified by a second-order tensor:

$$E = \begin{bmatrix} \frac{\partial u}{\partial x} & \frac{1}{2}\left(\frac{\partial u}{\partial y} + \frac{\partial v}{\partial x}\right) \\ \frac{1}{2}\left(\frac{\partial u}{\partial y} + \frac{\partial v}{\partial x}\right) & \frac{\partial v}{\partial y} \end{bmatrix} = \begin{bmatrix} e_{11} & e_{12} \\ e_{21} & e_{22} \end{bmatrix} \text{and}$$
$$\Omega = \begin{bmatrix} 0 & \frac{1}{2}\left(\frac{\partial u}{\partial y} - \frac{\partial v}{\partial x}\right) \\ -\frac{1}{2}\left(\frac{\partial u}{\partial y} - \frac{\partial v}{\partial x}\right) & 0 \end{bmatrix} = \begin{bmatrix} 0 & \omega \\ -\omega & 0 \end{bmatrix} \quad (3)$$

Here E is a kind of symmetric matrix representing the strain tensor and Ω is a kind of anti-symmetric matrix indicating the rigid body rotational change of motion (Teza and Galgaro 2008). The full description of the required results in terms of extensional strain, compression stain, and rotation rate has been discussed in the next section ("Spatial strain and rotation rate" section).

We applied a consistent relationship of M_w and m_b from Scrodilis (2006), which has been applied to analyse the global earthquake dataset with 20,870 earthquakes during the period of 1965 – 2003:

$$M_w = 0.85\ (\pm 0.04)\ m_b + 1.03\ (\pm 0.23)\ ;\ 3.5 \le m_b \le 6.2 \quad (4)$$

We converted all m_b earthquake events into Mw by using the global empirical relationship of Eq. 4 and calculated seismic moment (m_o) from moment magnitude (M_w) to assume the releasing moment from single and all earthquakes in the temporal variation by using Eq. 5 (Kanamori 1977):

$$M_w = \frac{2}{3}\log_{10} m_0 - 10.7 \quad (5)$$

Result and discussion

The outcomes of the study are discussed in terms of Eurasia-fixed reference frame (EUREF) velocity and ARIMA model-predicted values. The investigation of strain analysis and rotation rate in the PKB zone due to EUREF velocities is focused here. Finally, we presented a moment tensor inversion analysis of the earthquake mechanism that occurred in the Lower Silesia province of Poland on 21 July 2018 for the mainshock.

GNSS velocity field

The position and velocity of the GNSS stations are estimated as explained above in EUREF 2014 using the GAMIT–GLOBK postprocessing software (Herring et al. 2018). EUREF 2014 observed velocities of these GNSS stations along with a 95% confidence interval has been shown in Table 1. These velocities with uncertainties replicate the lithospheric crustal deformation in PKB and surrounding region (Fig. 3). As we can see from Table 1, the velocity and azimuth direction of the GNSS sites located in PKB such as CR01 (6.91 mm/yr; N51.52°), CR02 (6.43 mm/yr; N50.87°), CR06 (6.19 mm/yr; N57.34°), and CR11 (8.73 mm/yr; N63.46°), excluding CR05 (2.04 mm/yr N100.15°) (maybe some errors in data) showed almost 6.5 mm/yr average velocity and N50.0° average azimuth direction. The GNSS sites located in the MN unit characterised by velocities at CN02 (6.29 mm/yr), CS08 (2.46 mm/yr), NIWK (5.26 mm/yr), and WDZA (4.39 mm/yr) with N58.33°, N66.70°,

N64.65°, and N67.06° azimuth directions respectively, showed almost 4 mm/yr average velocities and N64.0° average azimuth directions. The stations CR4N (4.69 mm/yr; N236.04°) in PKB located at the Trzy Korony Mountain and the CS01 (8.92 mm/yr; N59.41°) in MN unit located at the Luban Mountain, stood out with some unexpected velocities, probably cause some local deformation. The remaining stations in the MN unit showed a decrement in absolute velocities and an increment in azimuth directions. Several studies have been conducted in this area and concluded that these kinds of changes in the lithosphere occurred because of thrusting which was accompanied by macroscopic fold formation with NNE-SSW to NE-SW trending fold axes. Folding occurred at comparatively greater depths with the development of cleavage formed by pressure solution (Bučová et al. 2010). The higher velocity in the PKB unit compared to the MN unit indicates a kind of compression. This compression is mainly oriented perpendicular to the strike of the PKB belt and recently oriented NW–SE direction (Bučová et al. 2010). The oldest brittle tectonic stages with E-W to NW–SE oriented maximum compression formed mainly reverse, oblique reverse, and strike-slip faults. These tectonic processes were accompanied by the relative counterclockwise (CCW) rotation of the Central Western Carpathian block with respect to Europe, which generated a dextral transpression zone along the western sector of the PKB in the Late Oligocene-Early Miocene (Fodor 1995; Marko et al. 2005).

We checked the EUREF velocities for the PF unit and found that the GNSS sites KACI (5.14 mm/yr; N59.89°); CS04 (6.21 mm/yr; N56.15°); CS07 (7.08 mm/yr; N47.52°); KAWI (4.49 mm/yr; N64.57°); and HAGA (5.13 mm/yr; N64.38°) showed small variation with the different locations. Janik et al. (2009) studied the PKB zone in southeast Poland and identified the boundaries between different crustal elements such as Pieniny lower, middle, and upper crust in deep seismic profiles. Similar kind of boundaries in the Eastern and Western Carpathians (PF and MN units) by several authors using refraction and wide-angle reflection celebration experiments (Grad et al. 2006; Janik et al. 2011; Starostenko et al. 2013; Hrubcová and Środa 2015). The nature of these boundaries was uncertain by them but there was the possibility that they are related to a thrust between older and younger crustal units (Gawęda et al. 2019). Long-term GNSS velocities variation in the current study, which confirmed their belonging with the active thrusting and folding as we mentioned above, is a kind of a clear sign of the slip-along tectonic activities which cause the regional deformation.

We modelled the estimated EUREF velocities by the ARIMA method to eliminate noise errors and improve the quality of time series velocities (Table 1). This modelling is intended to predict the long-term velocity time series and analyse the secular lithospheric deformation in PKB and the surrounding regions. During the ARIMA modelling, we excluded the CR04 and CR4N, because they have negative velocities which can be a cause of error in modelling. To distinguish the effect of the ARIMA model, the observed and modelled velocities have been shown in the same figure with distinct colours (Fig. 3). The residual between ARIMA modelled and EUREF observed velocity in PKB at CR01 (−0.235 mm/yr), CR02 (−0.238 mm/yr), CR06 (0.035 mm/yr), and CR11 (−0.29 mm/yr), indicates similar modelled and observed velocity field. The obtained results point out that the ARIMA model is successfully able to predict (within ~0.3 mm/yr) observed velocities in PKB. The residual velocity in MN unit is such as CS01 (−0.06 mm/yr), CN02 (−0.34 mm/yr), NIWK (−0.07 mm/yr), and WDZA (−1.71 mm/yr). Similarly, the residual for PF unit KACI (−0.62 mm/yr), CS04 (−0.35 mm/yr), CS07 (−0.12 mm/yr), KAWI (0.05 mm/yr), HAGA (−0.29 mm/yr), and GUBA (−1.86 mm/yr). As we can see, most of the velocity vectors match each other in the study area, except for those which contain discontinuities due to the tectonic phenomenon. The residuals between both velocities have a maximum difference of −1.71 mm/yr at WDZA in the MN unit and −1.86 mm/yr at GUBA in the PF unit; this is possible because of a small level of brittle deformation. Bučová et al. (2010) mentioned that the thrusting and folding in this region are followed by brittle deformation. ARIMA modelled velocity is the lowest at CR04 (~0.15 mm/yr) and the highest at CS01 (8.86 mm/yr), indicating an 8.71 mm/yr difference along all units. This type of difference points out some crustal slip along the active thrusts and folds and is able a cause regional deformation. This suggests the possibility of existing local intraplate activities among the PKB, MN, and PF units.

Spatial strain and rotation rate

We used the EUREF velocity field in the 2D version of the grid strain (strain_zero) programme written by Teza and Galgaro (2008) and estimated spatial strain rate variations in the PKB zone from 2004 to 2020. These strain rate variations at the selected GNSS stations have been plotted with red colour (extension) and blue colour (compression) as shown in Fig. 4 (Table S2, Supplementary file). The positive values are the sign of extension, and negative values are the sign of compression values. The rate of rotation at each GNSS station has been plotted with black colour as shown in Fig. 5. We estimated strain rates by using the above programme and noticed that the minimum and maximum extensional rates in PKB were around $1.04\times10^{-9}\pm4.9\times10^{-10}$/yr and $6.48\times10^{-9}\pm9.5\times10^{-10}$/yr respectively. The compressional rate has been estimated at around $5.00\times10^{-9}\pm1.58\times10^{-9}$/yr in the central region (selected region) of PKB while

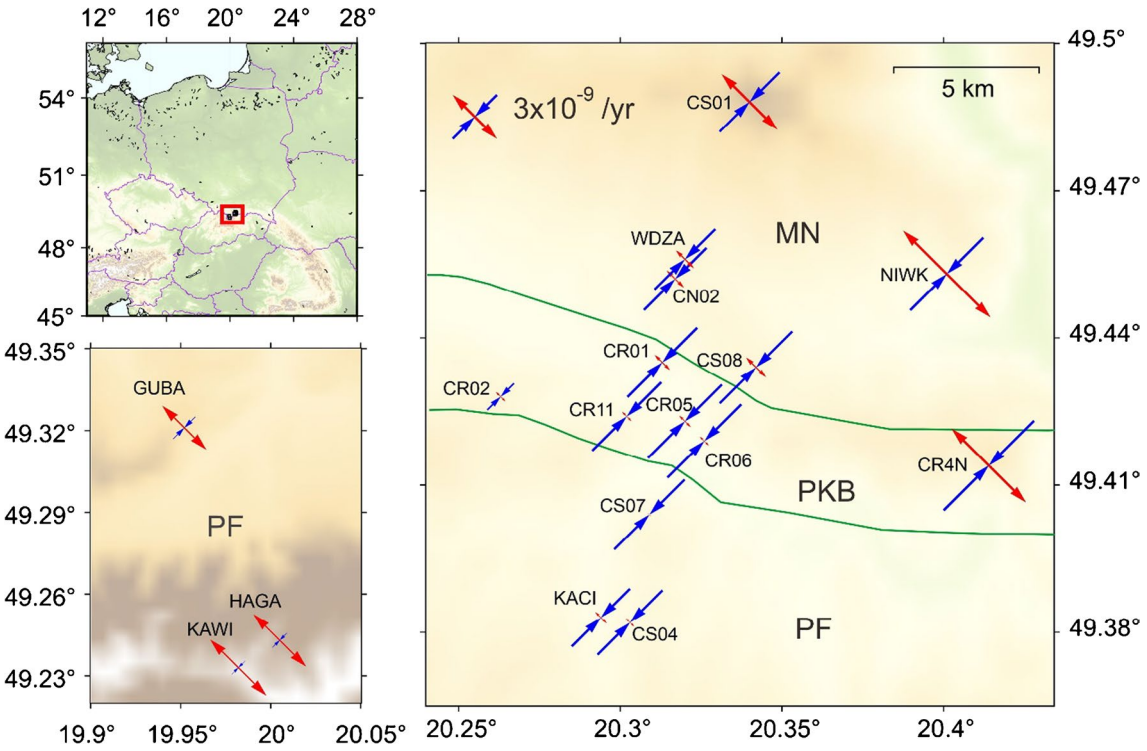

Fig. 4 Spatial strain variation in PKB zone from 2004 to 2020. The extension strain rates are presented with red arrows, while compression arrows are indicated by blue arrows

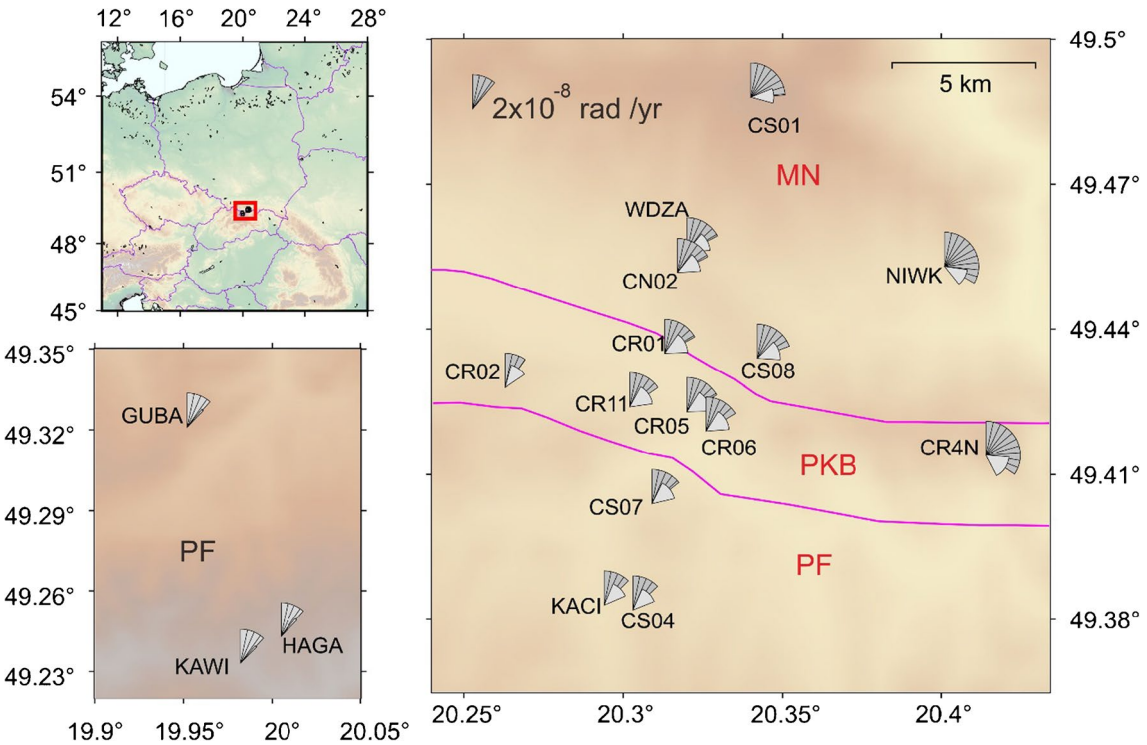

Fig. 5 Rotational rate in PKB zone Japan from 2004 to 2020. The rotational strain at each location of the GNSS site is denoted by black symbols

it has a very low value of $1.80\times10^{-9}\pm1.86\times10^{-9}$/yr in the western region (CR02) and very high value $6.10\times10^{-9}\pm5.76\times10^{-10}$/yr in the eastern region (CR4N) of PKB. This indicates that the strain rate in PKB varies from the western to the eastern part. If we talk about the rotational rates in PKB, they show a counterclockwise (CCW) pattern similar to the strain rates (Fig. 5). This CCW rotation rate is minimum around $1.77\times10^{-8}\pm1.02\times10^{-8}$ rad/yr (CR02) in the western part and maximum $6.17\times10^{-8}\pm1.46\times10^{-8}$ rad/yr (CR4N) in the western part. Márton et al. (2013) studied upper Cretaceous red marks and western Carpathian's new paleomagnetic results of the PKB and noticed the same kind of CCW rotations at both edges of the PKB. These CCW rotations are visible by Miocene period remagnetized rocks and suggest that the PKB was rotated in the CCW direction with a large angle during the period of Miocene. This also sets a constraint of time on the presumed oroclinal bending, which must be remagnetized predating the Miocene period. Bazhenov et al. (1980) performed the same kind of study on Upper Cretaceous red marls of PKB in western Slovakia and Poland. They concluded that PKB curvature was acquired in post-early Campanian time, which may be possible during the Neogene. However, the recent studies of the Paleogene and Cretaceous rocks north of PKB did not find any structural arc formation evidence during Neogene tectogenesis in Outer Carpathians (Márton et al. 2013).

The decreasing magnitude of the velocity in the MN units compared to PKB has already been discussed in the previous section. The strain rates are estimated in the MN units, and it has been found that the current accumulation rate is characterised by the dominant rate of contraction. The distribution of principal strain axes showed a normal contraction from $1.22\times10^{-8}\pm5.11\times10^{-9}$/yr to $1.17\times10^{-8}\pm4.94\times10^{-9}$/yr at the boundary of PKB. This is possible because of compressed force which works at the boundaries between PKB and MN units. A considerable clockwise rotation (CW) around $3.10\times10^{-8}\pm1.22\times10^{-8}$ rad/yr occurred in the MN unit at the boundary of part of PKB and enhanced up to $3.45\times10^{-8}\pm1.21\times10^{-8}$ rad/yr (Fig. 5). Although the velocity magnitude of NIWK site was low compared to CS01, their estimated strain and rotation rate at NIWK are high ($5.92\times10^{-9}\pm2.47\times10^{-9}$/yr extension, $4.95\times10^{-9}\pm4.39\times10^{-10}$/yr compression, and $5.97\times10^{-8}\pm1.08\times10^{-8}$ rad/yr rotation) compared to CS01 which shows $3.79\times10^{-9}\pm4.96\times10^{-9}$/yr extension, $4.06\times10^{-9}\pm1.49\times10^{-9}$/yr compression, and $4.32\times10^{-8}\pm9.25\times10^{-9}$ rad/yr rotation rates. This CCW rotation is a possible effect of inter-plate coupling alongside the MN unit. Regarding PF units at the sites (KACI, CS04, and CS07), the extensional rates are a little bit low (around $5.85\times10^{-10}\pm3.36\times10^{-10}$) while the extensional rate and rotation rate are almost equivalent to PKB unit. There are other studies that have been conducted in this region that claim that the MN discloses a uniform 50° CCW rotation along its strike (Márton et al. 2013). The Silesian nappe displays the same kind of CCW rotation except for the western side. This CCW rotation wrenches striped left lateral in the entire unit other than a uniform bending (Márton et al. 2009). Paleomagnetic outcomes from Neogene and Paleogene basins located in the eastern and western parts of Central Western Carpathians also support fairly uniform CCW rotation (Márton et al. 2013).

In contrast to the above regions, the estimated strain rate at the GNSS sites, such as GUBA, KAWI, and HAGA located in the Tatra mountains, is totally opposite to the other sites. Here extensional rates are high, and compression rates are low while the above region's extensional was low and compression was high (Table S2, Supplementary file). The maximum extension rate at these sites has been calculated as around $3.82\times10^{-9}\pm2.41\times10^{-10}$/yr, while the minimum extensional strain rate at the eastern side is estimated around $1.22\times10^{-9}\pm5.11\times10^{-10}$/yr. The average clockwise (CW) rate of rotation has been recorded around $2.06\times10^{-8}\pm1.43\times10^{-9}$ rad/yr in the Tatra mountains. Several other studies have shown moderate CW in the Tatra mountains (Kruczyk et al. 1992; Grabowski et al. 2010). This rotation pattern less or more follows the Carpathian arc demonstrating a possible oroclinal bending. In this context, the Paleogene–Neogene paleomagnetic outcomes must have occurred during Late Cretaceous orogeny. Most likely these regional components are formed during the Miocene age because their directions are similar to the reversed polarity magnetization of Neogene andesite intrusions from the Pieniny areas (Márton et al. 2004), as well as with secondary magnetization from the PKB segment of Poland (Grabowski et al. 2008).

Moment tensor inversion using Bayesian multiple chain method

The seismicity plot inside Poland and surrounding countries already has been shown in Fig. 1. There are two clusters of felt earthquakes inside Poland that occurred in the last decades, the first on 11 November 2015 (main shock Mw 3.7) and the second on 20 July 2018 (main shock Mw 5.0 Mw). We analysed the earthquake mechanism that occurred in the Lower Silesia province on 20 July 2018 using moment tensor inversion for the mainshock with the seismic stations from GE (Geofone Seismic Network), II (IRIS Seismic Network), CZ (Czech Seismic Network), DK (Danish Seismic Network), CH (Switzerland Seismic Network), and PL (Poland Seismic Network) in the distance up to 1000 km from the epicentre (Fig. 6). The inversion was performed for three rotating components of the seismogram (Z, Radial, and Transversal) using a probabilistic earthquake source inversion framework namely Grond (Heimann et al. 2018).

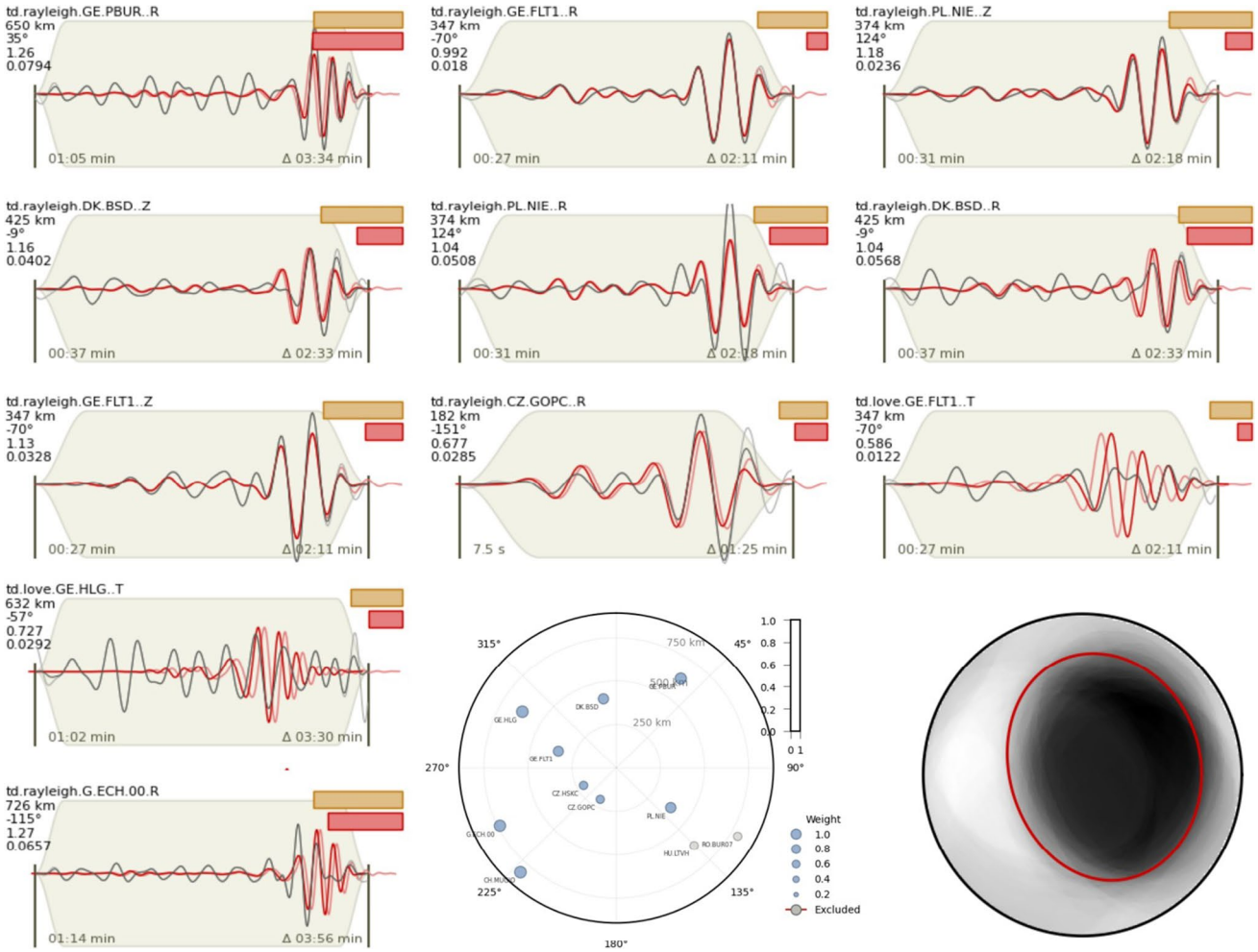

Fig. 6 The waveforms fitting results of the Mw 4.8 Lower Silesia earthquake on 21 July 2018. The figure shows the best and mean moment tensor solutions and their decomposition. Composite focal spheres are obtained by superposing the ensemble of solutions obtained by bootstrap. Examples of waveform fits: black seismograms correspond to observations, red ones to synthetics, the text reports the name of the seismic station, spatial component, epicentral distance, azimuth, maximum amplitude, and weight of each observation. The sphere diagram is the distance and azimuth position of the seismic stations that used in this research. The focal mechanism is the final results of the earthquake with thrusting mechanism

The Grond tool uses the Bayesian bootstrap optimization to explore the full model space and parameter uncertainties and efficiently solve the nonlinear optimization problem. The method begins by finding the model space by considering the samples from a uniform distribution within the bounds of given parameters and in parallel the evaluations of bootstrap are realised. The proposed distribution for newer models (focal parameters, moment magnitude, and centroid locations) using displacement waveforms independently and gradually updates based on the performance of tested models, until they convert equal or smaller to the continuously estimated updates of the distributed parameters and has a stable value with high confidence level. Moreover, an adaptive station weighting was applied simultaneously for individual stations based on the data error statistics (Kühn et al. 2020; Cabieces et al. 2020). Bayesian technique in global scale has been widely applied to study an assessment of a blind fault evidence (Simanjuntak and Ansari 2022, 2024); for example, Muksin et al., (2023) studied a blind backthrust active fault in North Sumatra that has generated a Mw 5.3 earthquake. It was similar scale of moderate magnitude with this study. Simanjuntak and Ansari (2023) studied an offshore unidentified active fault with Mw 7.3 using same method and found specific cluster with different focal mechanism.

Since the appropriate 1-D seismic velocity in the Poland region was not studied before, we verified Green's functions of the moment tensor inversion by using the pre-calculated velocity model (Heimann et al. 2019). The seismic moment and centroid parameters were simultaneously solved with fitted full displacement waveforms as usually used in the routine observational processing. We applied a bandpass filter of 0.03–0.06 for the 2018's earthquake. A total of

2000 different data configurations were given with 70,000 iterations to implement the Bayesian bootstrapping as the optimization process that ultimately produces stable convergence to the seismic source parameter solutions and source parameter uncertainties. The optimization explores a set of perturbed configuration models simultaneously and provides a well-fitting model that presents a posterior parameter probability along with the best solutions. The total of configurations and iterations is the trial-and-error procedure to assess the good quality of the focal mechanism from observed and synthetic waveform comparison which is quantitatively measured by the global (final) misfit value and guarantees the good convergence of the various models given. We estimated the 2018's earthquake with a stable magnitude (Mw) of 4.70 ± 0.01, depth of 6.0 ± 2 km, and duration of 3.7 ± 1.1 s. All parameters derived performed a low deviation and 60.80% confidence level, and the deviatoric component includes a compensated linear vector dipole (CLVD) component of $10 \pm 2\%$ while a double couple (DC) with $90\% \pm 3\%$. The result of the inversion for the 2018 earthquake resolved a thrusting mechanism with nodal plane 1 has a strike of 346°, dip of 32°, and rake of 92° while nodal plane 2 has a strike of 163°, dip of 58°, and rake 89°. However, the seismicity in the Poland region has experienced less significant earthquakes in the last century. It can be stated that less seismicity is reasonable due to the low slip rate from geodetic monitoring.

Conclusions

The study investigates active deformation to improve the current understanding of tectonic activities in the PKB and the surrounding region, i.e., Magura Nappe (MN) and Podhale Flysch (PF) units. We used 18 global navigation satellite system (GNSS) campaign mode stations located in this region for 16 years (2004–2020) of observations. Finally, the Bayesian inversion was applied to figure out the earthquake mechanism that occurred in the Lower Silesia province on 20 July 2018 using moment tensor inversion for the mainshock and largest aftershock with the seismic stations in the distance up to 1000 km from the epicentre. Long-term GNSS velocity variation in the current study confirmed their belonging with the active thrusting and folding. This is a clear sign of the slip-along tectonic activities which cause the regional deformation. The residual between EUREF and modelled by the ARIMA method indicates a possibility of a small level of brittle deformation. The distribution of principal strain axes showed a normal contraction at the boundary of PKB. This is possible because of the compressed force which works at the boundaries between PKB and MN units. A considerable counterclockwise rotation (CCW) occurred in the MN unit at the boundary of part of PKB point, a possibility of the effect of inter-plate coupling alongside the MN unit. In contrast to the above regions, the estimated strain rate at the GNSS in the Tatra mountains was totally opposite to the other sites, showing moderate counterclockwise rotation (CW) in the Tatra mountains. The result of the inversion for the 2018 Lower Silesia earthquake resolved a thrusting mechanism with a magnitude Mw of 4.70 ± 0.01, depth of 6.0 ± 2 km, and duration of 3.7 ± 1.1 s.

Supplementary Information The online version contains supplementary material available at https://doi.org/10.1007/s12517-024-11983-8.

Acknowledgements We thank our colleagues from the Department of Geodesy and Geodetic Astronomy at Warsaw University of Technology for providing us with observational data from many years of GNSS measurements at the Pieniny Klippen Belt.

Funding The research was funded by the Warsaw University of Technology within the Excellence Initiative: Research University (IDUB) programme.

Data availability The data that support the findings of this study are available on request from the corresponding author, [Kutubuddin Ansari], upon reasonable request.

Declarations

Conflict of interest The authors declare no competing interests.

References

Alexandrowicz SW (1993) Late Holocene molluscan assemblages from Czorsztyn (Pieniny Klippen Belt, Southern Poland). Folia Malac 5:15–24. https://doi.org/10.12657/folmal.005.001

Ansari K (2018) Crustal deformation and strain analysis in Nepal from GPS time-series measurement and modeling by ARMA method. Int J Earth Sci 107(8):2895–2905. https://doi.org/10.1007/s00531-018-1633-7

Ansari K, Bae TS (2020) Contemporary deformation and strain analysis in South Korea based on long-term (2000–2018) GNSS measurements. Int J Earth Sci 109(1):391–405. https://doi.org/10.1007/s00531-019-01809-4

Ansari K, Park KD (2019) Contemporary deformation and seismicity analysis in Southwest Japan during 2010–2018 based on GNSS measurements. Int J Earth Sci 108(7):2373–2390. https://doi.org/10.1007/s00531-019-01768-w

Ansari K, Park KD (2022) Geodetic analysis inside the South Korean Peninsula and impact of the 2011 Tohoku–Oki (TO) earthquake.

Acta Geologica Sinica - English Edition 96(2):631–647. https://doi.org/10.1111/1755-6724.14885
Ansari K, Corumluoglu O, Panda SK (2017) Analysis of ionospheric TEC from GNSS observables over the Turkish region and predictability of IRI and SPIM models. Astrophys Space Sci 362(4). https://doi.org/10.1007/s10509-017-3043-x
Barlik M (1998) Final report of the CERGOP Study Group 7 "CERGOP Gravity Network". Reports on Geodesy, (10/40), pp 235–241
Bazhenov M, Began A, Birkenmajer K, Burtman VS (1980) Paleomagnetic evidence of the tectonic origin of the curvature of the West Carpathian Arc. Bulletin de l'Académie Polonaise des Sciences. Series des Sciences de Terre 28/4, 281–290
Birkenmajer K (1974) Carpathian Mountains. Geol Soc Lond Spec Publ 4(1):127–157. https://doi.org/10.1144/GSL.SP.2005.004.01.0
Birkenmajer K (1986) Stages of the structural evolution of the Pieniny Klippen Belt, Carpathians. Studia Geol Pol 88:7–32
Bogdanova S, Gorbatschev R, Grad M, Janik T, Guterch A, Kozlovskaya E, Motuza G, Skridlaite G, Starostenko V, Taran L, EUROBRIDGE and POLONAISE Working Groups (2006) EUROBRIDGE: new insight into the geodynamic evolution of the East European Craton. Geol Soc Lond Memoirs 32(1):599–625. https://doi.org/10.1144/GSL.MEM.2006.032.01.3
Bruneton M, Pedersen HA, Farra V, Arndt NT, Vacher P, Achauer U, Alinaghi A, Ansorge J, Bock G, Friederich W, Grad M (2004) Complex lithospheric structure under the central Baltic Shield from surface wave tomography. J Geophys Res: Solid Earth 109(B10). https://doi.org/10.1029/2003JB002947
Bučová J, Plašienka D, Mikuš V (2010) Geology and tectonics of the Vršatec klippen area (Pieniny Klippen Belt, western Slovakia). In: Proceedings of the XIX Congress of the CBGA, Thessaloniky, Greece. Scientific Annals, School of Geology, Aristotle University of Thessaloniky, Spec, vol 100, pp 197–207
Cabieces R, Buforn E, Cesca S et al (2020) Focal parameters of earthquakes offshore Cape St. Vincent using an amphibious network. Pure Appl Geophys 177:1761–1780. https://doi.org/10.1007/s00024-020-02475-3
Czarnecki K, Barlik M, Czarnecka K, Olszak T, Pachuta A, Szpunar R, Walo J (2005) Geodynamic studies of the Pieniny Klippen Belt in the Czorsztyn region in 2001–2003. Acta Geodynamica Et Geomaterialia 2(3):33
Dadlez R, Grad M, Guterch A (2005) Crustal structure below the Polish Basin: is it composed of proximal terranes derived from Baltica? Tectonophysics 411(1–4):111–128. https://doi.org/10.1016/j.tecto.2005.09.004
Drewnik M (2006) The effect of environmental conditions on the decomposition rate of cellulose in mountain soils. Geoderma 132(1–2):116–130. https://doi.org/10.1016/J.GEODERMA.2005.04.023
Fodor L (1995) From transpression to transtension: Oligocene-Miocene structural evolution of the Vienna basin and the East Alpine-Western Carpathian junction. Tectonophysics 242(1–2):151–182. https://doi.org/10.1016/0040-1951(94)00158-6
Gawęda A, Golonka J, Waśkowska A, Szopa K, Chew D, Starzec K, Wieczorek A (2019) Neoproterozoic crystalline exotic clasts in the Polish Outer Carpathian flysch: remnants of the Proto-Carpathian continent? Int J Earth Sci 108:1409–1427. https://doi.org/10.1007/s00531-019-01713-x
Gibowicz SJ, Niewiadomski J, Wiejacz P, Domanski B (1989) Source study of the Lubin, Poland, mine tremor of 20 June 1987. Acta Geophys Pol 37(2):111–132
Grabowski J, Krobicki M, Sobień K (2008) New palaeomagnetic results from the Polish part of the Pieniny Klippen Belt, Carpathians-evidence for the palaeogeographic position of the Czorsztyn Ridge in the Mesozoic. Geol Q 52:31–44
Grabowski J, Michalik J, Pszczółkowski A, Lintnerova O (2010) Magneto-, and isotope stratigraphy around the Jurassic/Cretaceous boundary in the Vysoká Unit (Malé Karpaty Mountains, Slovakia): correlations and tectonic implications. Geol Carpath 61(4):309–326
Grad M, Polkowski M, Ostaficzuk SR (2016) High-resolution 3D seismic model of the crustal and uppermost mantle structure in Poland. Tectonophysics 666:188–210. https://doi.org/10.1016/j.tecto.2015.10.022
Grad M, Guterch A, Keller GR, Janik T, Hegedűs E, Vozár J, Ślączka A, Tiira T, Yliniemi J (2006) Lithospheric structure beneath trans-Carpathian transect from Precambrian platform to Pannonian basin: CELEBRATION 2000 seismic profile CEL05. J Geophys Res: Solid Earth 111(B3). https://doi.org/10.1029/2005JB003647
Guterch B, Lewandowska-Marciniak H, Niewiadomski J (2005) Earthquakes recorded in Poland along the Pieniny klippen belt, Western Carpathians. Acta Geophysica Polonica 53(1):27–45
Heimann S, Isken M, Kühn D, Sudhaus H, Steinberg A, Vasyura-Bathke H, Daout S, Cesca S, Dahm T (2018) Grond—a probabilistic earthquake source inversion framework. V. 1.0. GFZ Data Services. https://doi.org/10.5880/GFZ.2.1.2018.003
Heimann S, Vasyura-Bathke H, Sudhaus H, Isken MP, Kriegerowski M, Steinberg A, Dahm T (2019) A python framework for efficient use of pre-computed Green's functions in seismological and other physical forward and inverse source problems. Solid Earth 10(6):1921–1935. https://doi.org/10.5194/se-10-1921-2019
Herring T, King R, Floyd M, McClusky S (2018) Introduction to GAMIT/GLOBK, Release 10.7. http://www-gpsg.mit.edu/. Accessed 29 Dec 2019
Hrubcová P, Środa P (2015) Complex local Moho topography in the Western Carpathians: indication of the ALCAPA and the European Plate contact. Tectonophysics 638:63–81. https://doi.org/10.1016/j.tecto.2014.10.013
Jamrichová M, Józsa Š, Aubrecht R, Schlögl J (2012) Lower Cretaceous palaeokarst in a klippe of the Czorsztyn succession north of Zázrivá (Pieniny Klippen Belt, Orava sector, northern Slovakia). Acta Geol Slovaca 4(1):75–90
Janik T, Grad M, Guterch A (2009) Seismic structure of the lithosphere between the East European Craton and the Carpathians from the net of CELEBRATION 2000 profiles in SE Poland. Geol Q 53:141–158
Jurewicz E (2005) Geodynamic evolution of the Tatra Mts. and the Pieniny Klippen Belt (Western Carpathians): problems and comments. Acta Geol Polonica 55(3):295–338
Kacprzak A, Derkowski A (2007) Cambisols developed from coverbeds in the Pieniny Mts. (southern Poland) and their mineral composition. Catena 71(2):292–297. https://doi.org/10.1016/j.catena.2007.01.004
Kanamori H (1977) The energy release in great earthquakes. J Geophys Res 82(20):2981–2987. https://doi.org/10.1029/JB082i020p02981
Kruczyk J, Kadzialko-Hofmokl M, Lefeld J, Pagač P, Túnyi I (1992) Paleomagnetism of Jurassic sediments as evidence for oroclinal bending of the Inner West Carpathians. Tectonophysics 206(3–4):315–324
Kühn D, Heimann S, Isken MP, Ruigrok E, Dost B (2020) Probabilistic moment tensor inversion for hydrocarbon-induced seismicity in the Groningen Gas Field, The Netherlands, Part 1: testing. Bull Seismol Soc Am 110(5):2095–2111. https://doi.org/10.1785/0120200099
Lasocki S (2005) Probabilistic analysis of seismic hazard posed by mining induced events. In: Proc. 6th Int. Symp. on Rockburst in Mines "Controlling Seismic Risk". ACG, Perth, pp 151–156
Li J, Miyashita K, Kato T, Miyazaki S (2000) GPS time series modeling by autoregressive moving average method: application to the crustal deformation in central Japan. Earth Planet Space 52:155–162

Lizurek G (2017) Full moment tensor inversion as a practical tool in case of discrimination of tectonic and anthropogenic seismicity in Poland. Pure Appl Geophys 174:197–212. https://doi.org/10.1007/s00024-016-1378-9

Lizurek G, Plesiewicz B, Wiejacz P, Wiszniowski J, Trojanowski J (2013) Seismic event near Jarocin (Poland). Acta Geophysica 61(1):26–36. https://doi.org/10.2478/s11600-012-0052-6

Lizurek G, Rudziński Ł, Plesiewicz B (2015) Mining induced seismic event on an inactive fault. Acta Geophys 63:176–200. https://doi.org/10.2478/s11600-014-0249-y

Margański S (1997) The geodynamical test field in the Pieniny Klippen Belt. Przegląd Geodezyjny 8:10–13

Marko F, Vojtko R, Plašienka D, Sliva Ľ, Jablonský J, Reichwalder P, Starek D (2005) A contribution to the tectonics of the Periklippen zone near Zázrivá (Western Carpathians). Slovak Geol Mag 11(1):37–43

Márton E, Grabowski J, Plašienka D, Túnyi I, Krobicki M, Haas J, Pethe M (2013) New paleomagnetic results from the Upper Cretaceous red marls of the Pieniny Klippen Belt, Western Carpathians: evidence for general CCW rotation and implications for the origin of the structural arc formation. Tectonophysics 592:1–13

Márton E, Tokarski AK, Halasz DÓRA (2004) Late Miocene counterclockwise rotation of the Pieniny andesites at the contact of the Inner and Outer Western Carpathians. Geologica Carpathica 55(5):411–419

Márton E, Rauch-Włodarska M, Krejčí O, Tokarski AK, Bubík M (2009) An integrated palaeomagnetic and AMS study of the Tertiary flysch from the Outer Western Carpathians. Geophys J Int 177(3):925–940

Muksin U, Arifullah A, Simanjuntak AV, Asra N, Muzli M, Wei S, Gunawan E, Okubo M (2023) Secondary fault system in Northern Sumatra, evidenced by recent seismicity and geomorphic structure. J Asian Earth Sci 245:105557. https://doi.org/10.1016/j.jseaes.2023.105557

Mukul M, Jade S, Ansari K, Matin A (2014) Seismotectonic implications of strike-slip earthquakes in the Darjiling-Sikkim Himalaya. Curr Sci 106(2):198–210

Mukul M, Jade S, Ansari K, Matin A, Joshi V (2018) Structural insights from geodetic global positioning system measurements in the Darjiling-Sikkim Himalaya. J Struct Geol 114:346–356. https://doi.org/10.1016/j.jsg.2018.03.007

Nau R (2014) The mathematical structure of ARIMA models. Duke University 1(1):1–8

Niemyska-Lukaszuk J, Miechówka A, Zaleski T (2002) Gleby Pieninskiego Parku Narodowegoiich zagrozenia. Pieniny Przyroda i Człowiek 7:79–90

Plesiewicz B, Wiszniowski J (2015) Seismicity of Polish part of the Western Carpathians in the light of recent data. In: Guterch B, Kozák J (eds) Studies of historical earthquakes in Southern Poland. GeoPlanet: Earth and Planetary Sciences. Springer, Cham. https://doi.org/10.1007/978-3-319-15446-6_4

Qi Y, Feng W, Zhnag Y, Wang D, Du Y, Samsonov SV, Zhang P, Zaray AH, Ansari A (2023) Fault geometry, slip distribution and potential triggering of the 2022 MW 6.3 deadly Afghanistan earthquake revealed from geodetic and weather data. Seismol Res Lett 94(3):1–13. https://doi.org/10.1785/0220220341

Rudziński Ł, Cesca S, Lizurek G (2016) Complex rupture process of the March 19, 2013, Rudna mine (Poland) induced seismic event and collapse in the light of local and regional moment tensor inversion. Seismol Res Lett 87(2). https://doi.org/10.1785/0220150150

Scordilis EM (2006) Empirical global relations converting M S and m b to moment magnitude. J Seismol 10(2):225–236. https://doi.org/10.1007/s10950-006-9012-4

Simanjuntak AVH, Ansari K (2022) Seismicity clustering of sequence phenomena in the active tectonic system of backthrust Lombok preceding the sequence 2018 earthquakes. Arab J Geosci 15(23). https://doi.org/10.1007/s12517-022-10973-y

Simanjuntak AVH, Ansari K (2023) Spatial time cluster analysis and earthquake mechanism for unknown active fault (Kalatoa fault) in the Flores Sea. Earth Sci Inf 16:2649–2659. https://doi.org/10.1007/s12145-023-01067-8

Simanjuntak AVH, Ansari K (2024) Multivariate hypocenter clustering and source mechanism of 2017 Mw 6.2 and 2019 Mw 6.5 in the South Seram subduction system. Geotech Geol Eng. https://doi.org/10.1007/s10706-024-02780-x

Starostenko V, Janik T, Kolomiyets K, Czuba W, Środa P, Grad M, Kovács I, Stephenson R, Lysynchuk D, Thybo H, Artemieva IM (2013) Seismic velocity model of the crust and upper mantle along profile PANCAKE across the Carpathians between the Pannonian Basin and the East European Craton. Tectonophysics 608:1049–1072. https://doi.org/10.1016/j.tecto.2013.07.008

Teza G, Galgaro A (2008) Grid_strain and grid_strain3: sofware packages for strain feld computation in 2D and 3D environment. Comput Geosci 34(9):1142–1153

Walo J, Prochniewicz D, Olszak T, Pachuta A, Andrasik E, Szpunar R (2016) Geodynamic studies in the Pieniny Klippen Belt in 2004–2015. Acta Geodynamica Et Geomaterialia 13(4):351–361

Wiejacz P, Dębski W (2009) Podhale Poland earthquake of November 30 2004. Acta Geophysica 57(2):346–366. https://doi.org/10.2478/s11600-009-0007-8

Wilde-Piórko M, Świeczak M, Grad M, Majdański M (2010) Integrated seismic model of the crust and upper mantle of the Trans-European Suture zone between the Precambrian craton and Phanerozoic terranes in Central Europe. Tectonophysics 481(1–4):108–115. https://doi.org/10.1016/j.tecto.2009.05.002

Ząbek Z, Barlik M, Margański S, Pachuta A, Wojciechowski J (1988) Geodynamical investigations in the Pieniny klippen belt, Poland, from 1978 to 1985. Acta Geoph Polonica 36:2

Ząbek Z, Barlik M, Knap T, Margański S, Pachuta A (1993) Continuation of geodynamic investigations in the Pieniny Klippen Belt, Poland, from 1985 to 1990. Acta Geophys Polonica 41(2):131–150

Zuchiewicz W (1995) Selected aspects of neotectonics of the Polish Carpathians. Folia Quaternaria 66:145–204